

Identifying Patient-Specific Root Causes with the Heteroscedastic Noise Model

Eric V. Strobl, Thomas A. Lasko

Abstract—Complex diseases are caused by a multitude of factors that may differ between patients even within the same diagnostic category. A few underlying *root causes* may nevertheless initiate the development of disease within each patient. We therefore focus on identifying *patient-specific* root causes of disease, which we equate to the sample-specific predictivity of the exogenous error terms in a structural equation model. We generalize from the linear setting to the *heteroscedastic noise model* where $Y = m(X) + \varepsilon\sigma(X)$ with non-linear functions $m(X)$ and $\sigma(X)$ representing the conditional mean and mean absolute deviation, respectively. This model preserves identifiability but introduces non-trivial challenges that require a customized algorithm called Generalized Root Causal Inference (GRCI) to extract the error terms correctly. GRCI recovers patient-specific root causes more accurately than existing alternatives.

Index Terms—Causal inference, functional causal model, heteroscedastic noise, root cause

1 INTRODUCTION

CAUSAL inference refers to the process of inferring causal relationships from data. Randomized controlled trials (RCTs) remain the gold standard for causal inference in most fields of science. However, RCTs cannot distinguish between causes and *root causes* of disease, or the initial perturbations that ultimately induce a diagnostic label. Randomization also introduces a myriad of ethical, financial and logistical issues – such as withholding potentially lifesaving treatments from patients. We therefore instead focus on identifying root causes from *observational data*, where patients are not subject to randomization.

Consider for example the causal process depicted by the directed graph in Figure 1, where nodes represent random variables and directed edges their direct causal relations. The blue lightning bolt depicts an exogenous “shock” to the causal process, such as the effect of a somatic mutation or a virus, at $X_2 \in \mathbf{X}$. The shock is felt by many downstream variables X_3, \dots, X_6 and ultimately induces a diagnostic label $D = 1$. We focus on identifying X_2 from data because it corresponds to the initial perturbation and therefore the root cause. The problem is challenging because the root cause may lie arbitrarily far from D , and we must differentiate it from the other variables in \mathbf{X} that may be causes but not necessarily the root cause of the diagnosis.

The problem is further complicated by the fact that complex diseases may have *multiple* root causes that even *differ* between patients within the same diagnostic category.

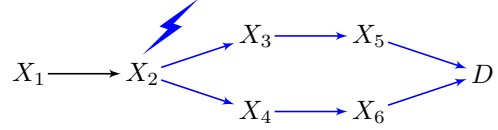


Fig. 1: Intuitive illustration of the difference between a cause and patient-specific root cause.

As a result, simply identifying root causes at the group level can lead to many statistically significant variables with clinically insignificant effect sizes. We instead focus our efforts on identifying *patient-specific* root causes in order to make complex diseases more tractable.

We identify patient-specific root causes by first defining a causal process using a structural equation model (SEM), where variables are related by a series of deterministic equations and stochastic error terms. Patient-specific root causes then correspond to the predictivity of the exogenous errors as assessed by sample-specific Shapley values (see Section 5 for details). Authors have thus far only implemented this idea in the linear case [1]. However, real datasets frequently contain non-linear relations, and running linear algorithms on data sampled from a non-linear SEM can lead to large errors in causal inference.

In this paper, we generalize to the non-linear setting as follows:

- (1) We identify patient-specific root causes using the *heteroscedastic noise model* (HNM) given by $Y = m(X) + \varepsilon\sigma(X)$ with arbitrary non-linear functions m and σ representing the conditional mean and conditional mean absolute deviation (MAD), respectively (Section 3).
- (2) We prove identifiability of the full causal graph under HNM (Section 4).
- (3) We introduce a principled algorithm called Generalized Root Causal Inference (GRCI) that extracts the error terms of an SEM satisfying HNM and computes sample-specific Shapley values (Section 6).

Experiments highlight considerable improvements in accuracy compared to prior methods because GRCI correctly identifies the exogenous errors by flexibly accounting for nonlinear causal relations.

2 BACKGROUND

We define a causal process using a *structural equation model* (SEM), or a series of equations in the form:

$$Z_i = f_i(\text{Pa}(Z_i), E_i), \quad \forall Z_i \in \mathbf{Z}, \quad (1)$$

where $\text{Pa}(Z_i)$ denotes the *parents*, or direct causes, of Z_i . The set \mathbf{E} contains mutually independent error terms. We assume $\mathbb{E}(\mathbf{E}) = 0$ without loss of generality. A linear SEM admits the more specific form:

$$Z_i = \text{Pa}(Z_i)\beta_{\text{Pa}(Z_i)} + E_i, \quad \forall Z_i \in \mathbf{Z}, \quad (2)$$

where β denotes a matrix of coefficients.

A *directed graph* \mathbb{G} is a graph with a directed edge \rightarrow or \leftarrow between any two vertices in \mathbf{Z} . We have $Z_i \rightarrow Z_j$ in \mathbb{G} if $Z_i \in \text{Pa}(Z_j)$ or, equivalently, Z_j is a *child* or direct effect of Z_i : $Z_j \in \text{Ch}(Z_i)$. The *neighbors* of Z_i unify the parents and children: $\text{Ne}(Z_i) = \text{Pa}(Z_i) \cup \text{Ch}(Z_i)$. We more specifically write $\text{Pa}_{\mathbb{G}}(Z_i)$ to emphasize the underlying graph – likewise for the children and neighbors. A *sink node* is a vertex without children. A *directed path* from Z_i to Z_j refers to a sequence of directed edges from Z_i to Z_j . Z_i is an *ancestor* of Z_j , denoted by $Z_i \in \text{Anc}_{\mathbb{G}}(Z_j)$, when there exists a directed path from Z_i to Z_j ; we likewise say Z_j is a *descendant* of Z_i . The set $\text{Nd}_{\mathbb{G}}(Z_i)$ corresponds to the non-descendants of Z_i . A *cycle* occurs when $Z_i \in \text{Anc}_{\mathbb{G}}(Z_j)$, and we have $Z_j \rightarrow Z_i$. A directed graph is called a *directed acyclic graph* (DAG), if it does not contain cycles. An *augmented graph* \mathbb{G}' is a DAG over $\mathbf{Z} \cup \mathbf{E}$ such that $E_i \in \text{Pa}_{\mathbb{G}'}(Z_i)$ and $\text{Pa}_{\mathbb{G}'}(E_i) = \emptyset$ for all $E_i \in \mathbf{E}$. We provide an example of a directed graph in Figure 1 and its corresponding augmented graph in Figure 3.

The triple $\langle Z_i, Z_j, Z_k \rangle$ forms a *collider* in \mathbb{G} , if we have $Z_i \rightarrow Z_j \leftarrow Z_k$, and Z_i and Z_k are non-adjacent. Z_i and Z_j are *d-connected* given $\mathbf{W} \subseteq \mathbf{Z} \setminus \{Z_i, Z_j\}$ if there exists a path between the two vertices such that any collider on the path is an ancestor of \mathbf{W} and no non-collider on the path is in \mathbf{W} . Otherwise, Z_i and Z_j are *d-separated* given \mathbf{W} .

A density $p(\mathbf{Z})$ associated with a DAG \mathbb{G} factorizes according to the product of the conditional densities of each variable in \mathbf{Z} given its parents:

$$p(\mathbf{Z}) = \prod_{i=1}^p p(Z_i | \text{Pa}_{\mathbb{G}}(Z_i)).$$

Any distribution which factorizes according to the above equation also satisfies the *global Markov property* where d-separation between Z_i and Z_j given \mathbf{W} in \mathbb{G} implies conditional independence (CI) between Z_i and Z_j given \mathbf{W} [2]. We refer to the converse as *d-separation faithfulness*. The density $p(\mathbf{X})$ is *causally minimal* if no proper subset of \mathbb{G} also obeys the global Markov property. D-separation faithfulness implies causal minimality [3].

The *Kolmogorov complexity* of a finite binary string x , denoted by $K(x)$, is the length of the shortest self-delimiting binary program that generates x on a universal Turing machine and then halts. The universal Turing machine is not unique, but the Kolmogorov complexity between any two such machines only differs by at most a constant. Most equalities and inequalities in algorithmic information theory are therefore only understood up to a constant; the notation

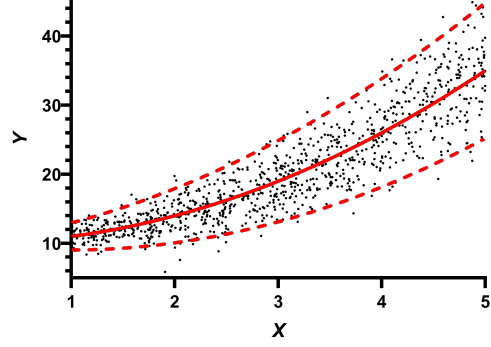


Fig. 2: Example of an HNM with $Y = X^2 + EX$ plus 10.

\pm means equality up to a constant and likewise \leq^+ for inequality.

To prevent cluttering of notation with too many parentheses, we write $p(Y)$ as p_Y when referring to the entire density. We keep the standard notation $p(y) = p(Y = y)$ when referring to a specific value of the density.

3 THE HETEROSCEDASTIC NOISE MODEL

3.1 Definition

We set $\mathbf{Z} = \mathbf{X} \cup D$, where D denotes a binary diagnostic label. We will have more to say about D in Section 5 and focus on \mathbf{X} for now. We can generalize the linear SEM in Equation (2) to an HNM SEM as follows:

Definition 1. (*Heteroscedastic noise model*) An SEM obeys the heteroscedastic noise model (HNM) if the following holds for each $X_i \in \mathbf{X}$:

$$X_i = m_i(\text{Pa}_{\mathbb{G}}(X_i)) + E_i \sigma_i(\text{Pa}_{\mathbb{G}}(X_i)), \quad (3)$$

for non-linear functions m_i and $\sigma_i > 0$.

We assume that $\mathbb{E}(\mathbf{E} | \text{Pa}_{\mathbb{G}}(X_i)) = 0$ and $\mathbb{E}(|\mathbf{E}| | \text{Pa}_{\mathbb{G}}(X_i)) = 1$ without loss of generality. HNM thus generalizes the linear SEM in Equation (2) by allowing the expectation and MAD (of the mean) to change as arbitrary non-linear functions of the parents.

Consider for example the bivariate HNM in Figure 2. The conditional expectation in solid red and conditional MAD in dashed red (at 95% prediction intervals) change as functions of X . In contrast, the best linear SEM erroneously fits a linear conditional expectation and assumes a constant variance. HNM thus increases modeling flexibility considerably.

3.2 Error-Term Extraction

We can extract the error terms \mathbf{E} from an HNM model using the Partial-Out algorithm summarized in Algorithm 1. The error term $E_i \in \mathbf{E}$ corresponds to:

$$E_i = \frac{X_i - m_i(\text{Pa}_{\mathbb{G}}(X_i))}{\sigma_i(\text{Pa}_{\mathbb{G}}(X_i))}. \quad (4)$$

The call $\text{Partial-Out}(\text{Pa}_{\mathbb{G}}(X_i), X_i)$ first estimates the conditional expectation $m_i(\text{Pa}_{\mathbb{G}}(X_i))$ by regressing X_i on $\text{Pa}_{\mathbb{G}}(X_i)$ in Line 1. Partial-Out optimizes all regression

Algorithm 1: Partial-Out

Input: \mathbf{V}, X_i **Output:** \hat{E}_i

- 1 $\hat{m}_i(\mathbf{V}), \hat{m}_i(\mathbf{V}) \leftarrow$ Regress X_i on \mathbf{V} with cross-validation
 - 2 $\hat{\sigma}_i(\mathbf{V}) \leftarrow$ Regress $|X_i - \hat{m}_i(\mathbf{V})|$ on \mathbf{V} with cross-validation
 - 3 Compute \hat{E}_i per Equation (5)
-

hyperparameters by cross-validation. The residuals correspond to:

$$X_i - \hat{m}_i(\text{Pa}_{\mathbb{G}}(X_i)) = E_i \sigma_i(\text{Pa}_{\mathbb{G}}(X_i)) + o_p(1),$$

where $\hat{m}_i(\text{Pa}_{\mathbb{G}}(X_i))$ denotes the estimate of the conditional expectation using a non-linear regression method. Let $\hat{m}_i(\text{Pa}_{\mathbb{G}}(X_i))$ denote the estimates of the conditional expectation on the validation folds with the best hyperparameter set. The algorithm then estimates the conditional MAD in Line 2 by regressing $|X_i - \hat{m}_i(\text{Pa}_{\mathbb{G}}(X_i))|$ on $\text{Pa}_{\mathbb{G}}(X_i)$ using the same folds as in Line 1 because:

$$\begin{aligned} & \mathbb{E}(|X_i - m_i(\text{Pa}_{\mathbb{G}}(X_i))| | \text{Pa}_{\mathbb{G}}(X_i)) \\ &= \sigma_i(\text{Pa}_{\mathbb{G}}(X_i)) \mathbb{E}(|E_i| | \text{Pa}_{\mathbb{G}}(X_i)) \end{aligned}$$

Care must be taken to regress on $|X_i - \hat{m}_i(\text{Pa}_{\mathbb{G}}(X_i))|$ and not $|X_i - \hat{m}_i(\text{Pa}_{\mathbb{G}}(X_i))|$ so that the training folds from Line 1 do not influence the validation folds in Line 2. We use the conditional MAD instead of the conditional standard deviation because we can directly estimate the conditional MAD and divide by it. Squaring the residuals in Step 2 to estimate the conditional variance and then taking its square root to obtain the conditional standard deviation can lead to large estimation errors in practice.

Partial-Out finally computes the error estimate in Line 3 as:

$$\hat{E}_i = \frac{X_i - \hat{m}_i(\text{Pa}_{\mathbb{G}}(X_i))}{\hat{\sigma}_i(\text{Pa}_{\mathbb{G}}(X_i))}, \quad (5)$$

per Equation (4). We *partial out* $\text{Pa}_{\mathbb{G}}(X_i)$ from X_i , when we compute \hat{E}_i by running $\text{Partial-Out}(\text{Pa}_{\mathbb{G}}(X_i), X_i)$ under HNM.

We implement all univariate regressions in practice using linear splines due to their relative robustness to overfitting and their ability to admit fast leave one out cross-validation using the Sherman–Morrison–Woodbury formula. We normalize all variables to $[0, 1]$ and then use m equispaced knots on $[0, 1]$ (always including 1 and replacing it with an offset). We choose m by leave one out cross-validation from 10 equispaced points between 2 and $\sqrt{n}/10$ inclusive, where n denotes the sample size. We generalize to multivariate regression by randomly projecting $t > 1$ variables onto $[0, 1]$ using $\sum_{i=1}^t w_i X_i$ with the vector \mathbf{w} obeying a Dirichlet distribution with alpha vector equal to all ones. This process ensures that we sample all weights uniformly from the $t - 1$ simplex, since we have no prior knowledge about the sparsity level.

4 IDENTIFIABILITY

We will use Partial-Out to extract the error terms from an SEM obeying HNM. The increased flexibility of accounting for heteroscedastic noise fortunately preserves *identifiability* of the model, or the ability to pinpoint the exact DAG when given the joint distribution.

We assume strictly positive densities throughout. We first have the following result in the bivariate case:

Theorem 1. Assume the forward model $X \rightarrow Y$ obeys HNM so that $p(x, y) = p(\frac{y - m(x)}{\sigma(x)})p(x)$ with $m(X)$ and $\sigma(X)$ once differentiable. If there is a backward model $Y \rightarrow X$ also obeying HNM so that $p(x, y) = p(\frac{x - n(y)}{t(y)})p(y)$, then the following differential equation holds:

$$\begin{aligned} & -\frac{\sigma(x)}{Q(x, y)} \frac{\partial^2}{\partial x \partial y} r(x, y) - \frac{\partial^2}{\partial y^2} r(x, y) + \\ & \frac{\sigma'(x)}{Q(x, y)} \frac{\partial}{\partial y} r(x, y) = q''(y) - \frac{\sigma'(x)}{Q(x, y)} q'(y), \end{aligned} \quad (6)$$

where $r(x, y) = \log p(\frac{x - n(y)}{t(y)})$, $q(y) = \log p(y)$ both twice differentiable and $Q(x, y) = \sigma(x)m'(x) + (y - m(x))\sigma'(x)$. Moreover, if there exists a quadruple $(x_0, m(x_0), \sigma(x_0), p(x_0|y))$ such that $Q(x_0, y) \neq 0$ for all but countably many y , then p_Y is completely determined by $(y_0, q'(y_0))$ – i.e., the set of all p_Y satisfying the differential equation is contained in a two dimensional affine space.

We delegate the longer proofs to the Supplementary Materials.

Equation (6) expresses a very specific relationship and suggests that finding a backward model satisfying the relation is like finding a needle in the haystack; we will almost never encounter this needle in practice. The statement that p_Y lies in a two dimensional space formalizes this intuition. It implies that the forward model cannot be inverted in general because the space of all possible p_Y is infinite dimensional *a priori*.

We recover the differential equation $-\frac{\sigma(x)}{Q(x, y)} \frac{\partial^2}{\partial x \partial y} r(x, y) - \frac{\partial^2}{\partial y^2} r(x, y) = q''(y)$ in the special case of an ANM with $\sigma'(x) = 0$ – thus replicating Lemma 1 in [4]. We can see that this relation holds when p_{XY} is Gaussian, a well-known case where we *cannot* identify the causal direction. We can of course just work out the equations with $Y = X\beta + \varepsilon_Y$: $-\frac{\sigma(x)}{Q(x, y)} \frac{\partial^2}{\partial x \partial y} r(x, y) \stackrel{+}{=} -\frac{1}{\beta} \frac{\beta}{\sigma_Y^2} = -\frac{1}{\sigma_Y^2}$, $\frac{\partial^2}{\partial y^2} r(x, y) \stackrel{+}{=} -\frac{1}{\sigma_Y^2}$ and $q''(y) = \frac{2}{\sigma_Y^2}$, so that Equation (6) holds in the Gaussian case. But more intuitively, Theorem 1 says that, if we are given information about X in terms of $(x_0, x_0\beta, \sigma_X, p(x_0|y))$, then we can recover p_Y with two points $(y_0, q'(y_0))$ when HNM holds in both directions. This of course holds in the Gaussian case because we can recover the entire (centered) bivariate density by only knowing $(\beta, \sigma_X, \sigma_Y)$.

The fact that p_Y is completely determined by just two parameters of Y when both directions hold suggests that $p_{X|Y}$ provides a substantial amount of information about p_Y . This conflicts with past work postulating that nature implements an *independence of causal mechanisms*, whereby $p_{X|Y}$ provides almost no information about p_Y [4], [5]. Authors rigorously define this information as follows:

Definition 2. (Algorithmic mutual information) Let s and t denote two binary strings. The algorithmic mutual information between s and t is:

$$I(s : t) = K(t) - K(t|s^*),$$

where s^* denotes the shortest program that computes s .

If $p_{X|Y}$ provides information about p_Y , then $K(p_Y|p_{X|Y}^*)$ is small, so we expect $I(p_Y : p_{X|Y}) \gg 0$.

The two parameter conclusion from Theorem 1 implies that $I(p_Y : p_{X|Y}) \gg 0$ in general under HNM. We can alternatively interpret Theorem 1 as follows: we must choose p_Y in a contrived fashion once we know $p_{X|Y}$, so that Equation (6) holds. The following theorem formalizes this intuition by showing that the complexity of p_Y indeed lower bounds $I(p_Y : p_{X|Y})$; in other words, if $I(p_Y : p_{X|Y}) \gg 0$, then p_Y is likely complex.

Theorem 2. Consider the same assumptions as Theorem 1. If both the forward and backward models follow HNM, then we have:

$$\begin{aligned} I(p_Y : p_{X|Y}) \\ \geq K(p_Y) - \inf_{(x_0, y_0)} K(x_0, m(x_0), \sigma(x_0), y_0, q'(y_0)), \end{aligned}$$

assuming of course that all inputs are computable.

The above theorem suggests that p_Y likely has high Kolmogorov complexity because $I(p_Y : p_{X|Y}) \gg 0$. This conclusion also dovetails nicely with complexity based approaches which posit that $K(p_X) + K(p_{Y|X}) \leq K(p_Y) + K(p_{X|Y})$ when $X \rightarrow Y$ [5], [6]. If both the forward and backward directions admit HNM, then the inequality is still likely to hold because $K(p_Y)$ is large. Finally, Theorem 2 connects with the main idea of the Information Geometric Causal Inference (IGCI) algorithm, where we can determine the causal direction $X \rightarrow Y$ when we can replace p_X with a simple density, such as the uniform or Gaussian density, but preserve the correlation between p_X and an arbitrary property of $p_{Y|X}$ [7], [8]. GRCI will go a step further than IGCI by determining both causal direction and the values of the error terms in order to compute patient-specific statistics.

GRCI will in particular extract the values of *all* of the error terms by partialing out the parents of each variable in \mathbf{X} . The algorithm thus requires identifiability of the entire causal graph \mathbb{G} , but Theorem 1 only applies to the bivariate case. We can fortunately extend Theorem 1 to the multivariate setting by considering the following definition:

Definition 3. (Restricted HNM) Equation (3) is a restricted HNM if, for all $Y \in \mathbf{X}$, $X \in \text{Pa}_{\mathbb{G}}(Y)$ and \mathbf{S} such that $(\text{Pa}_{\mathbb{G}}(Y) \setminus X) \subseteq \mathbf{S} \subseteq (\text{Nd}_{\mathbb{G}}(Y) \setminus X)$, there exists $\mathbf{S} = \mathbf{s}$ where $p(\mathbf{s}) > 0$ and $p(x, y|\mathbf{s})$ does not satisfy Equation (6).

In other words, Equation (6) does not hold when we condition on some value of the non-descendants of Y – notice that this is a very weak assumption. Let \mathcal{G} denote the space of all causally minimal DAGs obeying a restricted HNM. We have the following result:

Theorem 3. Assume Equation (3) is a restricted HNM according to \mathbb{G} . Then, \mathbb{G} is uniquely identified from \mathcal{G} .

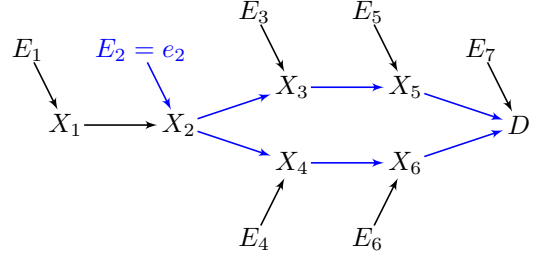


Fig. 3: The augmented graph of Figure 1. We represent the shock as a perturbation to the exogenous error term E_2 .

The proof reduces the multivariate model to a bivariate one and then applies a contradiction using Theorem 1. We conclude that the HNM model uniquely identifies the entire DAG as required for GRCI.

5 PATIENT-SPECIFIC ROOT CAUSES OF DISEASE

We want GRCI to compute patient-specific statistics to more specifically identify *patient-specific root causes of disease*, so we need to rigorously define the term. Consider a binary variable D denoting a diagnostic label of disease when $D = 1$ and healthy when $D = 0$. We assume that D is a sink node in \mathbb{G} ; this is a reasonable assumption because scientists who seek to identify the causes of D frequently measure phenomena like genomic levels or environmental exposures that are believed to precede the diagnosis in time.

A patient-specific root cause then corresponds to an exogenous shock to an otherwise healthy causal process that increases the probability that $D = 1$ as a downstream effect; we provided an example in Figure 1. We model this initial shock as a perturbation of the exogenous error term from a “healthy” value \tilde{e}_i to an “unhealthy” one e_i :

$$X_i = g_i(\text{Pa}_{\mathbb{G}}(X_i), E_i = \tilde{e}_i \xrightarrow{e_i}).$$

The unhealthy value affects downstream variables and increases the probability that $D = 1$ (Figure 3).

We quantify the *marginal* contribution of E_i to the increase in probability that $D = 1$ using the following difference:

$$\gamma_{E_i \cup \mathbf{W}} = q[\mathbb{P}(D = 1|E_i, \mathbf{W})] - q[\mathbb{P}(D = 1|\mathbf{W})], \quad (7)$$

for some monotonic function q and $\mathbf{W} = \emptyset$. We set q to the identity function for GRCI. If E_i alone increases the probability that $D = 1$, then $\gamma_{E_i} > 0$ because $\mathbb{P}(D = 1|E_i) > \mathbb{P}(D = 1)$.

Complex diseases may however have *multiple* root causes that induce disease only when present in combination. For example, a single genetic perturbation may not lead to cancerous growth, but multiple perturbations often do. We therefore generalize Equation (7) to average over all possible *joint* effects of E_i with the other error terms $\mathbf{E} \setminus E_i$:

$$S_i = \frac{1}{p} \sum_{\mathbf{W} \subseteq (\mathbf{E} \setminus E_i)} \frac{1}{\binom{p-1}{|\mathbf{W}|}} \gamma_{E_i \cup \mathbf{W}}. \quad (8)$$

Average over all possible combinations of $\mathbf{E} \setminus E_i$

This is precisely the *Shapley value* because we average over $\gamma_{E_i \cup \mathbf{W}}$ for all possible combinations of the errors [9]. S_i

can thus be greater than zero, when the joint effect $\gamma_{E_i \cup W}$ is greater than zero but the marginal effect γ_{E_i} equals zero. The Shapley value is also a *sample-specific* random variable because we average over the error terms but not the samples; we specifically have $S_i = s_i$ for any given patient i when $E_i \cup W = e_i \cup w_i$ for all $W \subseteq (E \setminus E_i)$.

We are now ready to define a patient-specific root cause:

Definition 4. $X_i \in \mathbf{X}$ is a patient-specific root cause of D if $X_i \in \text{Anc}_{\mathbb{G}'}(D)$ and $S_i > 0$.

In other words, $X_i \in \mathbf{X}$ is a patient-specific root cause if it is a cause of D and its error predictably induces $D = 1$, where predictivity is defined using the Shapley value S_i . Moreover, S_i is defined for each variable in $X_i \in \mathbf{X}$, so a patient may have multiple root causes that lead to disease.

6 GENERALIZED ROOT CAUSAL INFERENCE

We now detail the GRCI algorithm that recovers patient-specific root causes of disease from data. We summarize GRCI in Algorithm 2.

6.1 Skeleton Discovery

Non-linear regressors can easily overfit in high dimensions. GRCI therefore first reduces the dimensionality of the necessary regressions in Step 1 by identifying the *skeleton* of \mathbf{X} , or the presence and absence of the directed edges in \mathbb{G} . GRCI uses an algorithm called Skeleton-Stable – the skeleton discovery procedure of the well-known PC-Stable algorithm which identifies the skeleton using a series of CI tests [10]. An edge is present between any two variables X_i and X_j in \mathbb{G} if and only if $X_i \not\perp\!\!\!\perp X_j | W$, where $W \subseteq \text{Pa}_{\mathbb{G}}(X_i)$ or $W \subseteq \text{Pa}_{\mathbb{G}}(X_j)$, under d-separation faithfulness [11]. Skeleton-Stable therefore tests whether X_i and X_j are conditionally independent given dynamically adjusted supersets of the parents. We skip further details of the algorithm, since they are not important for this paper.

6.2 Global Error Term Extraction

In Step 2, GRCI uses the skeleton identified by Skeleton-Stable to extract the error terms of \mathbf{X} with the Extract-Errors algorithm.

We have summarized Extract-Errors in Algorithm 3. Extract-Errors initializes M to the set of all variables in \mathbf{X} . The algorithm then iteratively removes a member from M in Line 6 and places it into N in Line 7 so that N ultimately contains a reverse partial-order of \mathbf{X} . Extract-Errors identifies the variable to remove from M in Step 5 using the Find-Sink algorithm.

Algorithm 2: Generalized Root Causal Inference (GRCI)

Input: \mathbf{X} , test set \mathcal{T}

Output: \mathcal{S}

- 1 $\hat{\mathbb{G}} \leftarrow \text{Skeleton-Stable}(\mathbf{X})$
 - 2 $E, N \leftarrow \text{Extract-Errors}(\mathbf{X}, \hat{\mathbb{G}})$
 - 3 Compute the matrix \mathcal{S} containing the estimated sample-specific Shapley values of each patient in \mathcal{T}
-

We summarize Find-Sink in Algorithm 4. Find-Sink identifies the variable whose parents are most independent of its residuals due to the following result:

Lemma 1. If $X_i \in M$ is a sink node, then $E_i \perp\!\!\!\perp X_j$ for all $X_j \in M \setminus X_i$.

Proof. E_i and X_j are d-separated in \mathbb{G}' for all $X_j \in M \setminus X_i$. The conclusion follows by the global Markov property. \square

The algorithm in particular runs Partial-Out on each variable $X_i \in M$ given its neighbors to recover the residuals R_i . Find-Sink then computes the mutual information score $\max_{X_j \in \text{Ne}_{\mathbb{G}}(X_i)} I(X_j; R_i)$ using the nearest neighbor technique proposed in [12]. A lower mutual information score indicates a higher degree of independence. Find-Sink logs all of the mutual information scores associated with M in T , and then identifies the sink node in Line 6 as the variable in M associated with the smallest score in T .

Extract-Errors then partials out the sink node S identified by Find-Sink in Line 8. The algorithm also removes edges adjacent to S in $\hat{\mathbb{G}}$. The neighborhoods of some of the variables in M change due to this step – denote these variables in M by U . Extract-Errors updates the scores in T for U in the next iteration. Repeating this process of identifying a sink node in M , partialing out its errors and placing it into N until M is empty results in (1) a reverse partial order in N and (2) all of the error terms collected in E . More formally:

Lemma 2. Extract-Errors recovers all of the error terms of \mathbf{X} .

Proof. We prove this induction. The base case follows by Lemma 1. For the induction step, assume that Extract-Errors recovers all error terms when $|M| = n$. We need to show that the statement holds for $n+1$. We can recover a sink node from M when $|M| = n+1$ by Lemma 1. The conclusion follows by the inductive hypothesis. \square

6.3 Shapley Values

GRCI finally computes the matrix \mathcal{S} containing the Shapley values in Step 3. The i^{th} column and j^{th} row of \mathcal{S} contains the Shapley value of $X_i \in \mathbf{X}$ for the patient j in test set \mathcal{T} . We compute these values in practice by predicting D with XGBoost using the error terms recovered by Extract-Errors and then applying the TreeSHAP algorithm [9], [13]. We certify GRCI with the following theorem:

Theorem 4. (Fisher consistency) Under d-separation faithfulness and HNM over \mathbf{X} , GRCI recovers the true Shapley values and therefore the patient-specific root causes of D for all samples in \mathcal{T} .

Proof. Skeleton-stable recovers a superset of the skeleton of \mathbb{G} under d-separation faithfulness [10]. Extract-Errors recovers all of the error terms of \mathbf{X} by Lemma 2. The mutual independence of the error terms and the exactness of the TreeSHAP algorithm ensure that the matrix \mathcal{S} contains the true Shapley values [9]. The conclusion follows for the entries in \mathcal{S} greater than zero by Definition 4. \square

Algorithm 3: Extract-Errors

Input: $X, \hat{\mathbb{G}}$
Output: E, N

```

1  $M, U \leftarrow X$ 
2  $N \leftarrow \emptyset$ 
3  $T \leftarrow \infty$ 
4 repeat
5    $S \leftarrow \text{Find-Sink}(M, U, T, \hat{\mathbb{G}})$ 
6    $M \leftarrow M \setminus S$ 
7    $N \leftarrow N \cup S$ 
8    $E_S \leftarrow \text{Partial-Out}(\text{Ne}_{\hat{\mathbb{G}}}(S), S)$ 
9    $U \leftarrow \text{members of } M \text{ adjacent to } S \text{ in } \hat{\mathbb{G}}$ 
10  Remove edges adjacent to  $S$  in  $\hat{\mathbb{G}}$ 
11 until  $M = \emptyset$ ;

```

Algorithm 4: Find-Sink

Input: $M, U, T, \hat{\mathbb{G}}$
Output: sink S

```

1 return  $M$  if  $|M| = 1$ 
2 for  $X_i \in U$  do
3    $R_i \leftarrow \text{Partial-Out}(\text{Ne}_{\hat{\mathbb{G}}}(X_i), X_i)$ 
4    $T_i \leftarrow \max_{X_j \in \text{Ne}_{\hat{\mathbb{G}}}(X_i)} I(X_j; R_i)$ 
5 end
6  $S \leftarrow M[\arg \min_{X_i \in U} T_i]$ 

```

6.4 Time Complexity

GRCI is composed of three steps as summarized in Algorithm 2. Skeleton-Stable in Step 1 calls a CI test at most $O(p^r)$ times, where r denotes the maximum number of neighbors of a vertex in \mathbb{G} . The CI test we implement performs a fixed number of multivariate adaptive spline regressions (MARS) each requiring $O(nrm^4)$ time, where n denotes the sample size and m the maximum number of basis functions [14].¹ Skeleton-Stable therefore requires $O(nrp^rm^4)$ time. The Extract-Errors function in Step 2 iterates twice over the variables, so it requires on the order of p^2 iterations. Each iteration is dominated by Partial-Out which requires $O(n^2b + b^3)$ time, where b denotes the maximum number of basis functions used during cross-validation. Extract-Errors therefore requires $O(n^2p^2b + p^2b^3)$ time. Finally, the TreeSHAP algorithm computes in $O(nltld^2)$ time, where t refers to the number of trees, l the maximum number of leaves, and d the maximum tree depth. Repeating this process for each of the p variables requires $O(nptld^2)$ time. GRCI thus ultimately requires $O(nrp^rm^4) + O(n^2p^2b + p^2b^3) + O(nptld^2)$ time. We conclude that GRCI scales quadratically with respect to sample size and polynomially $O(p^r)$ with respect to the number of variables if $r \geq 2$.

7 RELATED WORK

Authors have proposed to identify causal direction using functional forms more restrictive than HNM. For example, LiNGAM considers a linear SEM with non-Gaussian errors,

1. We replace random Fourier regression with MARS regression and use a fixed number of non-linear transformations similar to [15].

while ANM considers a nonlinear SEM with additive noise [16], [17]. The post-nonlinear model (PNL) assumes that the error can be made homoscedastic under a monotonic transformation of the response [18]. All of these models therefore only consider additive errors, whereas HNM allows both additive and multiplicative forms.

Recently, [19] also considered HNM and proposed an algorithm called HEC for determining causal direction in the bivariate case. HEC divides the range of the predictor variable into a finite set of bins and then fits an additive model in each bin. The authors additionally assume that the error terms follow a Gaussian distribution in order to optimize the number of bins using the BIC score. Another algorithm called Fourth Order Moment (FOM) assumes approximately Gaussian errors but allows the conditional variance to change in a smooth, rather than in a piece-wise, fashion [20]. GRCI in contrast admits a smooth conditional variance *and* allows the error term to admit an arbitrary, potentially non-Gaussian distribution.

Other methods, such as those proposed in [21]–[23], also allow heteroscedastic noise but determine causal direction *without* recovering the error terms. We therefore cannot use these algorithms to compute the Shapley values necessary for identifying patient-specific root causes of disease.

A third set of algorithms attempt to identify root causes rather than just determine causal direction. The RCI algorithm for example identifies patient-specific root causes of disease but assumes the LiNGAM model [1]. Unfortunately, we cannot simply substitute LiNGAM with HNM in RCI because *indirect* causal relations may not follow HNM even if Equation (3) holds – i.e., HNM is not closed under marginalization. Other authors defined patient-specific root causes as conditional outliers, but not all root causes are outliers and not all outliers induce disease [24]. We therefore instead define patient-specific root causes using Shapley values. A third algorithm identifies root causes by substituting certain causal conditionals into an SEM, but this method struggles to scale beyond several variables and identifies root causes at the population level rather than at the desired patient-specific level [25]. The root causes of complex diseases likely differ dramatically between patients, so we must identify *patient-specific* root causes in order to make complex diseases tractable.

In summary, GRCI improves upon previous work because it:

- (1) adopts the identifiable heteroscedastic noise model which includes both LiNGAM and ANM as special cases;
- (2) generalizes RCI to models that are not closed under marginalization, such as HNM and ANM;
- (3) identifies root causes at the patient-specific level in order to make complex diseases tractable.

8 EXPERIMENTS

Hyperparameters. GRCI requires two hyperparameters: the α value for Skeleton-Stable and the k value for the nearest neighbor mutual information estimator. We set α to the

liberal threshold of 0.1, which in practice causes Skeleton-Stable to output a superset of the true skeleton. This superset represents a small subset of the fully connected graph that greatly reduces the dimensionality of the regressions performed in Step 2.

We fixed $k = 10$ for the mutual information estimator for three reasons. First, the entropy estimate is consistent for any fixed value of k . The standard deviation of the estimator also stabilizes at $k = 10$ for most sample sizes according to Figure 4 of [12]. Moreover, the estimate is near exact when independence truly holds as shown in Figure 2 of [12]. Both of these experimental results hold for nearly all cases tested by the authors.

Reproducibility. All R code needed to replicate experimental results is available at github.com/ericstrobl/GRCI.

8.1 Causal Direction

GRCI computes a (reverse) partial ordering N , so we can use the algorithm to recover causal direction in the bivariate setting after assuming that an edge exists between X and Y . We compared GRCI against four algorithms on their ability to identify causal direction in the bivariate setting:

- (1) HETeroscedastic noise Causal model (HEC): bins X and fits a polynomial regressor in each bin while assuming intra-bin homoscedasticity. The algorithm chooses the causal direction as the one minimizing the BIC score [19].
- (2) Fourth Order Moment (FOM): estimates the fourth-order moment of the residuals using a heteroscedastic Gaussian process. The algorithm chooses the causal direction as the one minimizing the fourth-order moment [20].
- (3) REGression and Subsequent Independence Test (RESIT): assumes an ANM, regresses out the conditional mean using a Gaussian process and determines causal direction using a reproducing kernel-based conditional independence test [3].
- (4) Direct LiNGAM (DL): assumes variables are linearly related with non-Gaussian errors [26]. The algorithm decides causal direction using the differential entropy measure proposed in [27].

The first two algorithms cover state of the art methods that handle heteroscedastic noise. The other two algorithms are state of the art for the additive noise and linear non-Gaussian acyclic models. Other algorithms in the literature utilize information theoretic measures and do not impose functional forms. We however only compare against methods which can extract the values of the error terms, since we are ultimately interested in performing patient-specific root causal inference rather than just determining causal direction.

8.1.1 Synthetic Data

We generated data using three different functional models:

- (1) LiNGAM: $Y = X\beta + E$
- (2) ANM: $Y = f(X) + E$
- (3) HNM: $Y = f(X) + Eg(X)$,

with $f(X)$ and $g(X) - 1$ uniformly sampled from the set $\{\sqrt{X^2 + 1} - 1, X\Psi(X), 1/(1 + \exp(-X))\}$; we subtracted

one from $g(X)$ to ensure non-zero variance. We sampled the distribution of E uniformly from the following possibilities: uniform distribution on $[-1, 1]$, t-distribution with five degrees of freedom, chi square distribution with three degrees of freedom. Note that LiNGAM requires at least one non-Gaussian error, whereas ANM and HNM do not. We therefore also included the centered Gaussian distribution with variance $1/9$ as one of the possibilities for the error term of ANM and HNM. We repeated the above procedure 200 times for LiNGAM with non-Gaussian errors, 200 times for ANM with non-Gaussian errors and another 200 times with Gaussian errors, 200 times for HNM with non-Gaussian errors and another 200 times with Gaussian errors. We therefore generated a total of 1000 independent datasets.

We report the results in Figure 4. LiNGAM, GRCI and RESIT performed well under LiNGAM. Of course, LiNGAM and RESIT outperform GRCI in this case, because they are specifically designed for the homoscedastic setting. Only GRCI and RESIT performed well under ANM with non-Gaussian errors because LiNGAM assumes linear conditional expectations. GRCI, HEC and FOM all performed equivalently with Gaussian error terms under both ANM and HNM. However, GRCI outperformed the other two – sometimes by a very large margin – with non-Gaussian errors. Recall that HEC and FOM make a variety of Gaussian approximations which unfortunately do not work well in the non-Gaussian setting. Overall, GRCI achieves the best performance with an accuracy of 83.5% as compared to 71.0% for HEC, 72.8% for FOM, 69.9% for RESIT and 49.0% for DL. We conclude that GRCI maintains good performance across all conditions while other algorithms only perform well in certain cases. Timing results are located in the Supplementary Materials; GRCI completed within 0.4 seconds on average.

8.1.2 Real Data

The Tübingen cause-effect pairs benchmark contains 108 datasets of real cause-effect pairs [28]. We summarize the results for the 108 pairs in Figure 5. As is standard in the literature, we exclude pairs containing multivariate vectors or binary variables; this includes pair numbers 47, 52-55, 70, 71, 105 and 107. We evaluate accuracy using the suggested weighted average in order to account for the potential bias introduced by pairs derived from the same multivariable dataset. The x-axis in Figure 5 corresponds to the cause-effect pair number (1-108), and the y-axis to the moving weighted accuracy. An ideal algorithm should achieve the highest weighted accuracy at any pair number. GRCI obtained an overall weighted accuracy of 81.6%, as opposed to 71.2% for FOM, 70.5% for HEC, 64.0% for RESIT and 51.5% for LiNGAM. Interestingly, these results match the overall accuracy for the synthetic data to within a few percentage points. GRCI also maintained the best weighted accuracy at any pair number. We conclude that GRCI accurately discovers causal direction using real data. In general, algorithms that account for heteroscedasticity (GRCI, FOM, HEC) perform better than those that only account for homoscedasticity (RESIT, LiNGAM), and algorithms that account for non-linear relations (GRCI, FOM, HEC, RESIT) perform better than those that only account for linear relations (LiNGAM). Timing results are located

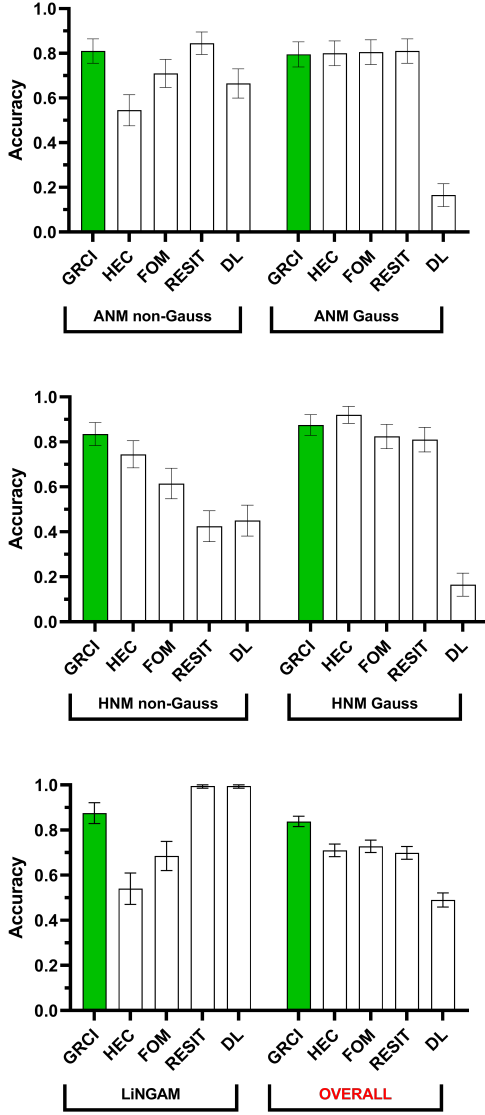


Fig. 4: Results on causal direction with synthetic data under different conditions. Rows correspond to functional model and columns to Gaussianity. Error bars denote 95% confidence intervals of the mean. GRCI performs well across all conditions while the other algorithms only perform well in some cases.

in the Supplementary Materials; GRCI completed within 5 seconds on average.

Summarizing the results of the causal direction experiments:

- (1) GRCI maintains good performance across LiNGAM, ANM and HNM, regardless of whether the errors are Gaussian or not.
- (2) HEC and FOM do not perform well when error terms deviate from Gaussianity.
- (3) GRCI obtains and maintains the best performance with real data.
- (4) The overall accuracy on the synthetic data almost

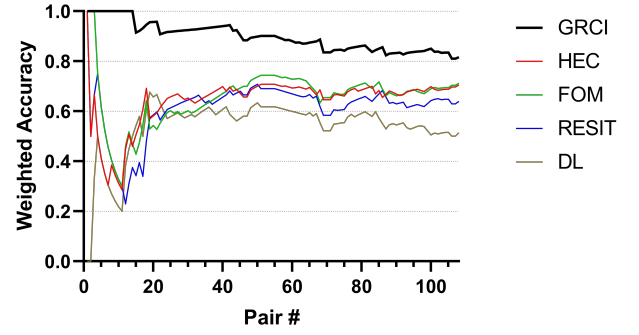


Fig. 5: Results on the 108 Tübingen cause-effect pairs. GRCI maintains the highest weighted accuracy at any pair number.

exactly mimics the final accuracy on the real data.

8.2 Root Causal Inference

We next investigate the performance of GRCI in discovering patient-specific root causes of disease. We compare against four other algorithms:

- (1) Root Causal Inference (RCI): recovers patient-specific root causes assuming that the joint distribution obeys the LiNGAM model [1].
- (2) Prediction with ICA (ICA): runs ICA and then ranks the identified sources using a local variable importance measure of random forest [29].
- (3) Conditional Outliers (CO): learns a causal graph \hat{G} and then identifies patient-specific root causes as conditional outliers according to the score $\frac{|X_i - m_i(\text{Pa}_{\hat{G}}(X_i))|}{\sigma_i(\text{Pa}_{\hat{G}}(X_i))}$ [24].
- (4) Model Substitution (MS): learns a causal graph and then identifies *group level* root causes by substituting causal conditional distributions into the joint distribution [25].

We equipped CO and MS with Partial-Order because the methods can adapt to different functional assumptions. Using linear methods as in [1] results in worse performance.

CO and MS also require a method for identifying the underlying causal graph. We tested RESIT and GDS as proposed in [3], but they did not scale even after substituting a fast non-parametric conditional independence test [15]. We therefore instead ran Steps 1 and 2 of GRCI to recover a partial order. The parents of a variable must precede it in the partial order. So we next ran Skeleton-Stable with conditioning sets restricted to preceding variables according to the partial order and then oriented directed edges according to the partial order. This process recovers a unique DAG. We fixed the alpha threshold to 0.05 because it led to the best results in our experiments.

Computing the ground truth Shapley values requires an exponential number of summations per Equation (8). We therefore instead estimated the ground truth to negligible error by (1) feeding XGBoost fifty thousand samples of the *ground truth* error terms and (2) running the TreeSHAP

algorithm on the learned model. We reran all applicable algorithms (RCI and ICA) using XGBoost and TreeSHAP in order to prevent GRCI from achieving an unfair advantage due to possible biases introduced during ground truth estimation.

8.2.1 Synthetic Data

We generated data from a DAG with an expected neighborhood size of two, $\mathbb{E}(N) = 2$. We assigned adjacencies using independent realizations of a Bernoulli($\frac{\mathbb{E}(N)}{p-1}$) random variable in an upper triangular matrix. We then replaced the binary variables twice with samples from Uniform($[-1, -0.25] \cup [0.25, 1]$). Let β^1 denote the first resultant coefficient matrix, and β_{ji}^1 to the j^{th} row and i^{th} column; likewise for β^2 . We generated the non-Gaussian error terms using the same procedure described in Section 8.1.1. The HNM model corresponds to $X_i = f_i(\sum_{X_j \in \text{Pa}_{\mathbb{G}}(X_i)} X_j \beta_{ji}^1) + E_i g_i(\sum_{X_j \in \text{Pa}_{\mathbb{G}}(X_i)} X_j \beta_{ji}^2)$ for each $X_i \in \mathbf{X}$ with functions f_i, g_i drawn randomly as in Section 8.1.1. We finally permuted the variable order. Repeating the above procedure 200 times for sample sizes of $n = 500, 1000, 2000$ and dimensions $p = 10, 30, 50$ generated a total of $200 \times 3 \times 3 = 1800$ datasets.

Metrics. Comparing the algorithms is not straightforward because the algorithms have different outputs. GRCI returns sample-specific Shapley values for all of the variables. RCI returns sample-specific Shapley values only for some of the variables, since it performs variable selection. ICA outputs sample-specific scores according to a random forest metric, but it can be modified to return sample-specific Shapley values for all of the variables. MS outputs *group-level* Shapley values, and CO outputs sample-specific conditional outlier scores both only for some of the variables. We need a method that compares the algorithms on a common footing and accounts for outputs of different lengths.

All algorithms fortunately can return a ranked list of variables. The top ranked variables ideally should correspond to the root causes with the largest effect on D . We therefore evaluated the algorithms using ranked-biased overlap (RBO) [30], a well-established metric that compares two ranked lists. Let \mathcal{R}^k , correspond to the ground truth ranking of the root causes for patient k according to the true Shapley values. Similarly let $\hat{\mathcal{R}}^k$ denote the estimate of the ranking given by an algorithm. The RBO corresponds to:

$$\frac{1}{n} \sum_{k=1}^n \sum_{i=1}^{q_k} \tilde{s}_i^k |\hat{\mathcal{R}}_{1:i}^k \cap \mathcal{R}_{1:i}^k| / i, \quad (9)$$

where s_i^k denotes the true Shapley value of X_i for patient k , $\tilde{s}_i^k = \frac{s_i^k}{\sum_{i=1}^{q_k} s_i^k}$ the version normalized to sum to one, and q_k the total number of root causes for patient k . RBO can compare ranked lists of potentially varying lengths and weighs top variables more heavily than bottom ones. The metric takes values between zero and one; it equals one when the top ranked variables coincide exactly between the two lists, and zero when there is no overlap. A higher RBO is therefore better.

GRCI, RCI and ICA also attempt to estimate the values of the error terms which directly impact the quality of the

p	n	GRCI	RCI	RCI _t	ICA	ICA _t	CO	MS
10	500	0.735	0.706	0.690	0.579	0.639	0.616	0.508
	1000	0.773	0.699	0.689	0.603	0.669	0.623	0.502
	2000	0.809	0.710	0.708	0.614	0.695	0.631	0.503
30	500	0.653	0.622	0.616	0.477	0.519	0.496	0.392
	1000	0.711	0.654	0.647	0.537	0.593	0.463	0.347
	2000	0.745	0.682	0.673	0.573	0.641	0.485	0.379
50	500	0.639	0.569	0.580	0.327	0.345	0.432	0.348
	1000	0.685	0.613	0.609	0.506	0.556	0.402	0.338
	2000	0.741	0.642	0.636	0.555	0.615	0.383	0.311

(a) RBO

p	n	GRCI	RCI	ICA
10	500	0.160	0.650	3.044
	1000	0.113	0.659	3.362
	2000	0.104	0.620	3.435
30	500	0.183	0.756	3.455
	1000	0.138	0.700	3.556
	2000	0.111	0.635	3.355
50	500	0.186	0.791	3.558
	1000	0.170	0.702	3.632
	2000	0.108	0.643	3.361

(b) MSE

p	n	GRCI	RCI	RCI _t	ICA	ICA _t	CO	MS
10	500	1.613	0.003	0.651	0.182	0.776	1.208	1.248
	1000	4.075	0.004	0.832	0.404	1.073	3.585	3.686
	2000	13.85	0.009	1.186	0.914	1.659	13.43	13.95
30	500	9.199	0.011	0.720	0.383	1.075	10.51	10.64
	1000	22.56	0.020	0.946	0.925	1.644	24.40	24.80
	2000	108.2	0.043	1.375	2.285	2.830	111.5	113.6
50	500	32.90	0.033	0.850	0.650	1.477	39.32	39.61
	1000	83.21	0.058	1.135	1.603	2.398	91.39	92.28
	2000	222.0	0.125	1.806	4.145	4.708	235.7	240.0

(c) Time in seconds

TABLE 1: GRCI obtains the highest mean RBO values in (a) and lowest mean MSE values in (b) in every situation tested with the synthetic data. All HNM-based algorithms take approximately the same amount of time to complete as highlighted in gray in (c).

estimated Shapley values. We therefore evaluated these algorithms using the mean squared error (MSE) to the ground truth error values as well:

$$\frac{1}{nw} \sum_{k=1}^n \sum_{i=1}^w (\hat{s}_i^k - s_i^k)^2,$$

where w denotes number of ground truth ancestors of D . We set $\hat{s}_i^k = 0$, if the algorithm does not output a score for variable i . A lower MSE is better.

Results. We summarize the accuracy results with the synthetic data using RBO and MSE in Tables 1 (a) and 1 (b), respectively. Recall that we implemented two versions of RCI and ICA - the original ones and the modified forms using TreeSHAP as labeled using the subscript t . We therefore compared GRCI against a total of six algorithms. Bolded values in each row of the tables correspond to the best performing algorithms according to paired two-tailed t-tests each at a Bonferonni corrected threshold of 0.05/6.

GRCI achieved the highest mean RBO in every situation (Table 1 (a)). The original version of RCI came in second place and TreeSHAP did not improve its performance. TreeSHAP improved ICA, but both versions of ICA performed

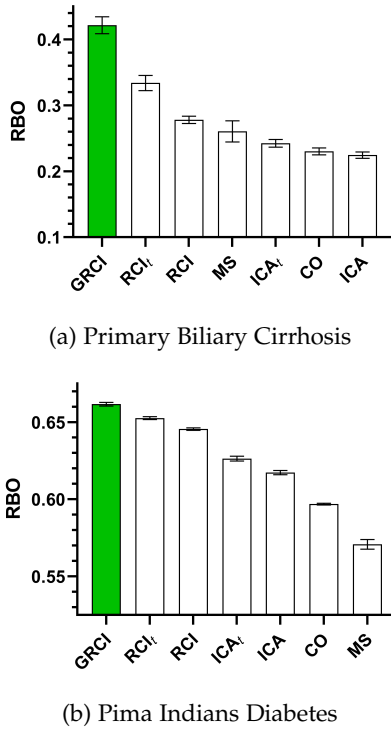


Fig. 6: Sorted accuracy results with the real datasets.

much worse than GRCI and RCI. ICA frequently got stuck in local optima as evidenced by the terribly inaccurate error values when compared to RCI (Table 1 (b)). GRCI recovered the error terms about two to six times more accurately than RCI. MS and CO had the worst performances because the algorithms either recovered conditional outliers that did not induce disease or failed to output sample-specific scores. We conclude that GRCI performs the most accurately across all tested sample sizes, dimensions and metrics even after incorporating TreeSHAP into applicable alternatives.

We summarize timing results in Table 1 (c). Algorithms that search over the space of HNMs – including GRCI, CO and MS highlighted in light gray – take about the same amount of time. These methods also expectedly take longer than the linear algorithms RCI and ICA.

8.2.2 Real Data

We compared all seven algorithms on their ability to discover patient-specific root causes using two real datasets. Note that we do not have access to the ground truth Shapley values with real data, so we use the following modified RBO metric:

$$\frac{1}{n} \sum_{k=1}^n \sum_{i=1}^{q_k} \frac{1}{q_k} |\hat{\mathcal{R}}_{1:i}^k \cap \mathcal{R}_{1:i}^k| / i,$$

where we no longer weight the score by Shapley values.

Primary Biliary Cholangitis. The Mayo Clinic Primary Biliary Cholangitis (PBC) dataset contains samples from 258 patients with PBC who entered into a randomized clinical trial assessing the effects of medication called D-penicillamine [31]. PBC is an autoimmune disease that slowly destroys the small bile ducts of the liver, eventually causing liver cirrhosis, liver decompensation and then death

[32]. The dataset contains the following continuous variables: age, bilirubin, albumin, alkaline phosphatase, copper, cholesterol, platelets, AST and pro-thrombin time.

We sought to identify the patient-specific root causes of mortality. We know that age and bilirubin cause death because older patients pass away and increased bilirubin leads to neurotoxicity [33]. Intervening on the other variables does not consistently change mortality, so they are likely non-ancestors of death. High levels of bilirubin increase the frequency of death more than old age. We set the gold standard ranking as bilirubin then age if the bilirubin is at or above 2 mg/dL – in accordance with the classic Child-Turcotte cut-off [34] – and bilirubin then age otherwise.

We ran the algorithms on 1000 bootstrapped draws of the dataset. We report accuracy results among patients who passed in Figure 6 (a). GRCI achieved the best accuracy compared to all other methods. RCI came in second place in accordance with the synthetic data results. GRCI took 8 seconds on average (see the Supplementary Materials for full timing results).

Pima Indians Diabetes. The Pima Indians Diabetes Database is a observational dataset containing samples from females in the Pima Indian population near Pheonix, Arizona [35]. The dataset contains the following variables: number of pregnancies, plasma glucose concentration at two hours in an oral glucose tolerance test, diastolic blood pressure, triceps skinfold thickness, two-hour serum insulin, body mass index, diabetes pedigree function, age, and presence or absence of diabetes.

We sought to identify the patient-specific root causes of diabetes. Recall that the incidence of diabetes increases with age, and clinicians can diagnose diabetes if the blood glucose reaches at least 200 mg/dL with a two hour oral glucose tolerance test. We therefore set the gold standard as age and glucose ranked according to their z-score in decreasing order.

We ran the algorithms again using 1000 bootstrapped draws. We reports the results for patients with diabetes in Figure 6 (b). GRCI again achieved the best accuracy compared to all other methods. The results with the Pima Indians Diabetes Database also mimic those seen with the PBC and synthetic datasets. GRCI took 15.2 seconds on average (Supplementary Materials).

Summarizing the results of the patient-specific root causal inference experiments:

- (1) GRCI achieves the best performance – in terms of both RBO or MSE – across all sample sizes and dimensions with the synthetic data.
- (2) GRCI also achieves the best performance in two real datasets with known root causes, and the real data results mimic the synthetic ones.
- (3) GRCI, MS and CO take longer than the linear algorithms but still complete within about 4 minutes on average with $n = 2000, p = 50$.

9 CONCLUSION

We presented GRCI, the first method that generalizes the original RCI algorithm to the non-linear setting. GRCI ac-

commodates both non-linear expectations and heteroscedastic noise under the HNM model. We proved identifiability of HNM in general and described a procedure that partials out both the conditional mean and MAD in a two-step regression process. We then rigorously defined patient-specific root causes using sample-specific Shapley values of the error terms. We introduced GRCI as an efficient method that recovers these errors by combining error extraction in functional causal models with constraint-based skeleton discovery. Experiments with both synthetic and real data highlighted considerable improvements in accurately recovering both causal direction and patient-specific root causes of disease. GRCI even outperformed other methods based on HNM engineered specifically for causal direction because GRCI does not make any Gaussian approximations.

REFERENCES

- [1] Strobl EV, Lasko TA. Identifying Patient-Specific Root Causes of Disease. arXiv preprint arXiv:220511627. 2022.
- [2] Lauritzen SL, Dawid AP, Larsen BN, Leimer HG. Independence properties of directed Markov fields. *Networks*. 1990;20(5):491-505.
- [3] Peters J, Mooij JM, Janzing D, Schölkopf B. Causal Discovery with Continuous Additive Noise Models. *Journal of Machine Learning Research*. 2014;15:2009-53.
- [4] Janzing D, Steudel B. Justifying additive noise model-based causal discovery via algorithmic information theory. *Open Systems & Information Dynamics*. 2010;17(02):189-212.
- [5] Janzing D, Schölkopf B. Causal inference using the algorithmic Markov condition. *IEEE Transactions on Information Theory*. 2010;56(10):5168-94.
- [6] Stegle O, Janzing D, Zhang K, Mooij JM, Schölkopf B. Probabilistic latent variable models for distinguishing between cause and effect. *Advances in Neural Information Processing Systems*. 2010;23.
- [7] Janzing D, Mooij J, Zhang K, Lemeire J, Zscheischler J, Daniušis P, et al. Information-geometric approach to inferring causal directions. *Artificial Intelligence*. 2012;182:1-31.
- [8] Janzing D, Steudel B, Shajarisales N, Schölkopf B. Justifying information-geometric causal inference. In: *Measures of Complexity*. Springer; 2015. p. 253-65.
- [9] Lundberg SM, Erion GG, Lee SI. Consistent individualized feature attribution for tree ensembles. arXiv preprint arXiv:180203888. 2018.
- [10] Colombo D, Maathuis MH. Order-independent constraint-based causal structure learning. *Journal of Machine Learning Research*. 2014;15(1):3741-82.
- [11] Spirtes P, Glymour CN, Scheines R, Heckerman D. *Causation, Prediction, and Search*. MIT Press; 2000.
- [12] Kraskov A, Stögbauer H, Grassberger P. Estimating mutual information. *Physical Review E*. 2004;69(6):066138.
- [13] Chen T, Guestrin C. XGBoost: A scalable tree boosting system. In: *Proceedings of the 22nd ACM SIGKDD International Conference on Knowledge Discovery and Data Mining*; 2016. p. 785-94.
- [14] Friedman JH. Multivariate adaptive regression splines. *The Annals of Statistics*. 1991;19(1):1-67.
- [15] Strobl EV, Zhang K, Visweswaran S. Approximate kernel-based conditional independence tests for fast non-parametric causal discovery. *Journal of Causal Inference*. 2019;7(1).
- [16] Shimizu S, Hoyer PO, Hyvärinen A, Kerminen A, Jordan M. A linear non-Gaussian acyclic model for causal discovery. *Journal of Machine Learning Research*. 2006;7(10).
- [17] Hoyer P, Janzing D, Mooij JM, Peters J, Schölkopf B. Nonlinear causal discovery with additive noise models. *Advances in Neural Information Processing Systems*. 2008;21.
- [18] Zhang K, Hyvärinen A. On the Identifiability of the Post-Nonlinear Causal Model. In: *25th Conference on Uncertainty in Artificial Intelligence (UAI 2009)*. AUAI Press; 2009. p. 647-55.
- [19] Xu S, Marx A, Mian O, Vreeken J. Causal Inference with Heteroscedastic Noise Models. *Proceedings of the AAAI Workshop on Information Theoretic Causal Inference and Discovery*. 2022.
- [20] Cai R, Ye J, Qiao J, Fu H, Hao Z. FOM: Fourth-order moment based causal direction identification on the heteroscedastic data. *Neural Networks*. 2020;124:193-201.
- [21] Tagasovska N, Chavez-Demoulin V, Vatter T. Distinguishing cause from effect using quantiles: Bivariate quantile causal discovery. In: *International Conference on Machine Learning*. PMLR; 2020. p. 9311-23.
- [22] Mitrovic J, Sejdinovic D, Teh YW. Causal inference via kernel deviance measures. *Advances in Neural Information Processing Systems*. 2018;31.
- [23] Liu F, Chan LW. Causal inference on multidimensional data using free probability theory. *IEEE transactions on neural networks and learning systems*. 2017;29(7):3188-98.
- [24] Janzing D, Budhathoki K, Minorics L, Blöbaum P. Causal structure based root cause analysis of outliers. arXiv preprint arXiv:191202724. 2019.
- [25] Budhathoki K, Janzing D, Bloebaum P, Ng H. Why did the distribution change? In: *International Conference on Artificial Intelligence and Statistics*. PMLR; 2021. p. 1666-74.
- [26] Shimizu S, Inazumi T, Sogawa Y, Hyvärinen A, Kawahara Y, Washio T, et al. DirectLiNGAM: A direct method for learning a linear non-Gaussian structural equation model. *Journal of Machine Learning Research*. 2011;12:1225-48.
- [27] Hyvärinen A, Smith SM. Pairwise likelihood ratios for estimation of non-Gaussian structural equation models. *Journal of Machine Learning Research*. 2013;14(Jan):111-52.
- [28] Mooij JM, Peters J, Janzing D, Zscheischler J, Schölkopf B. Distinguishing cause from effect using observational data: methods and benchmarks. *Journal of Machine Learning Research*. 2016;17(1):1103-204.
- [29] Lasko TA, Mesa DA. Computational Phenotype Discovery via Probabilistic Independence. *KDD Workshop on Applied Data Science for Healthcare*. 2019.
- [30] Webber W, Moffat A, Zobel J. A similarity measure for indefinite rankings. *ACM Transactions on Information Systems (TOIS)*. 2010;28(4):1-38.
- [31] Fleming TR, Harrington DP. *Counting Processes and Survival Analysis*. vol. 169. John Wiley & Sons; 2011.
- [32] Hirschfield GM, Gershwin ME. The immunobiology and pathophysiology of primary biliary cirrhosis. *Annual Review of Pathology: Mechanisms of Disease*. 2013;8:303-30.
- [33] López-Velázquez JA, Chávez-Tapia NC, Ponciano-Rodríguez G, Sánchez-Valle V, Caldwell SH, Uribe M, et al. Bilirubin alone as a biomarker for short-term mortality in acute-on-chronic liver failure: an important prognostic indicator. *Annals of Hepatology*. 2014;13(1):98-104.
- [34] Child CG. Surgery and portal hypertension. *The Liver and Portal Hypertension*. 1964:50-2.
- [35] Smith JW, Everhart JE, Dickson W, Knowler WC, Johannes RS. Using the ADAP learning algorithm to forecast the onset of diabetes mellitus. In: *Proceedings of the Annual Symposium on Computer Application in Medical Care*. American Medical Informatics Association; 1988. p. 261.

SUPPLEMENTARY MATERIALS

Proofs

Theorem 1. Assume the forward model $X \rightarrow Y$ obeys HNM so that $p(x, y) = p\left(\frac{y-m(x)}{\sigma(x)}\right)p(x)$ with $m(X)$ and $\sigma(X)$ once differentiable. If there is a backward model $Y \rightarrow X$ also obeying HNM so that $p(x, y) = p\left(\frac{x-n(y)}{t(y)}\right)p(y)$, then the following differential equation holds:

$$-\frac{\sigma(x)}{Q(x, y)} \frac{\partial^2}{\partial x \partial y} r(x, y) - \frac{\partial^2}{\partial y^2} r(x, y) + \frac{\sigma'(x)}{Q(x, y)} \frac{\partial}{\partial y} r(x, y) = q''(y) - \frac{\sigma'(x)}{Q(x, y)} q'(y),$$

where $r(x, y) = \log p\left(\frac{x-n(y)}{t(y)}\right)$, $q(y) = \log p(y)$ both twice differentiable and $Q(x, y) = \sigma(x)m'(x) + (y - m(x))\sigma'(x)$. Moreover, if there exists a quadruple $(x_0, m(x_0), \sigma(x_0), p(x_0|y))$ such that $Q(x_0, y) \neq 0$ for all but countably many y , then

p_Y is completely determined by $(y_0, q'(y_0))$ – i.e., the set of all p_Y satisfying the differential equation is contained in a two dimensional affine space.

Proof. We first derive the differential equation. Let $\pi(x, y) = \log p(x, y)$. The forward model allows us to write:

$$\begin{aligned}\frac{\partial \pi(x, y)}{\partial y} &= \frac{q' \left(\frac{y-m(x)}{\sigma(x)} \right)}{\sigma(x)} \\ \frac{\partial^2 \pi(x, y)}{\partial y^2} &= \frac{q'' \left(\frac{y-m(x)}{\sigma(x)} \right)}{\sigma^2(x)} \\ &= \frac{\overbrace{[\sigma(x)m'(x) + (y-m(x))\sigma'(x)]}^{=Q(x,y)}}{\sigma(x)} \frac{\partial^2 \pi(x, y)}{\partial y^2} \\ &+ \frac{\sigma'(x) \frac{\partial}{\partial y} \pi(x, y)}{\sigma(x)}.\end{aligned}$$

We can also write $\frac{\partial}{\partial y} \pi(x, y) = \frac{\partial}{\partial y} r(x, y) + q'(y)$ and likewise $\frac{\partial^2}{\partial y^2} \pi(x, y) = \frac{\partial^2}{\partial y^2} r(x, y) + q''(y)$ by the backward model.

Observe $\frac{\partial^2}{\partial y \partial x} \pi(x, y) = \frac{\partial^2}{\partial y \partial x} r(x, y)$. Hence we have:

$$\begin{aligned}\frac{\partial^2 r(x, y)}{\partial y \partial x} &= \frac{-Q(x, y) \left(\frac{\partial^2}{\partial y^2} r(x, y) + q''(y) \right)}{\sigma(x)} \\ &+ \frac{\sigma'(x) \left(\frac{\partial}{\partial y} r(x, y) + q'(y) \right)}{\sigma(x)}.\end{aligned}$$

Rearranging the above equation leads to Equation (6).

We now prove the second statement. Let $z(y) = q'(y)$, $G(x, y) = \frac{\sigma'(x)}{Q(x, y)}$ and:

$$\begin{aligned}H(x, y) &= -\frac{\sigma(x)}{Q(x, y)} \frac{\partial^2}{\partial x \partial y} r(x, y) - \frac{\partial^2}{\partial y^2} r(x, y) \\ &+ \frac{\sigma'(x)}{Q(x, y)} \frac{\partial}{\partial y} r(x, y).\end{aligned}$$

We may then write:

$$z'(y) = z(y)G(x, y) + H(x, y).$$

Solving this linear differential equation gives:

$$z(y) = ce^{\int G(x, \tilde{y}) d\tilde{y}} + e^{\int G(x, \tilde{y}) d\tilde{y}} \times \int e^{\int G(x, \tilde{y}) d\tilde{y}} H(x, \hat{y}) d\hat{y}, \quad (10)$$

for some arbitrary constant c . Now fix $(x_0, m(x_0), \sigma(x_0), p(x_0|y))$. Then the function $z(y)$ is determined for all y by y_0 and $z(y_0)$, so long as $Q(x_0, y) \neq 0$ for all but countably many y , because we can use y_0 and $z(y_0)$ to find the value of c (i.e., the initial condition of the solution). We can then recover $q(y)$ for all y by integration (the constant follows by normalization). Thus, the set of all functions p_Y satisfying Equation (6) is completely determined by y_0 and $q'(y_0)$ – a two dimensional affine space. \square

Theorem 2. Consider the same assumptions as Theorem 1. If both the forward and backward models follow HNM, then we have:

$$\begin{aligned}I(p_Y : p_{X|Y}) \\ \geq K(p_Y) - \inf_{(x_0, y_0)} K(x_0, m(x_0), \sigma(x_0), y_0, q'(y_0)),\end{aligned}$$

assuming of course that all inputs are computable.

Proof. Equation (10) implies that $q'(y)$ is completely determined by $(x_0, m(x_0), \sigma(x_0), y_0, q'(y_0))$ given $p_{X|Y}$. We can therefore write: $K(q'(y)|p_{X|Y}) \stackrel{+}{\leq} K(x_0, m(x_0), \sigma(x_0), y_0, q'(y_0)|p_{X|Y})$. This holds for arbitrary (x_0, y_0) , so we more specifically have:

$$K(q'(y)|p_{X|Y}) \stackrel{+}{\leq} \inf_{(x_0, y_0)} K(x_0, m(x_0), \sigma(x_0), y_0, q'(y_0)|p_{X|Y}).$$

Note that we can recover p_Y from q' by integration. The constant is determined by the normalization of a density. We can now write:

$$\begin{aligned}I(p_Y : p_{X|Y}) &= K(p_Y) - K(p_Y|p_{X|Y}^*) \\ &\stackrel{+}{\geq} K(p_Y) - K(p_Y|p_{X|Y}) \\ &\stackrel{+}{\geq} K(p_Y) - \inf_{(x_0, y_0)} K(x_0, m(x_0), \sigma(x_0), y_0, q'(y_0)|p_{X|Y}) \\ &\stackrel{+}{\geq} K(p_Y) - \inf_{(x_0, y_0)} K(x_0, m(x_0), \sigma(x_0), y_0, q'(y_0)),\end{aligned}$$

whence the conclusion holds. \square

Theorem 3. Assume Equation (3) is a restricted HNM according to \mathbb{G} . Then, \mathbb{G} is uniquely identified from \mathcal{G} .

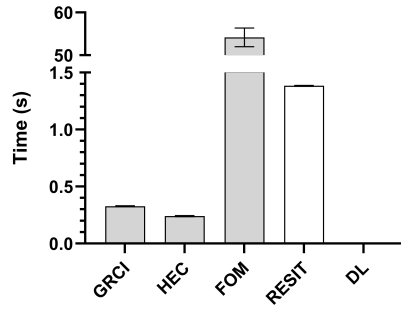
Proof. Assume that there exists another restricted HNM with graph $\underline{\mathbb{G}}$. We will show that $\mathbb{G} = \underline{\mathbb{G}}$ for any $\underline{\mathbb{G}} \in \mathcal{G}$. Assume $\mathbb{G} \neq \underline{\mathbb{G}}$. Since causal minimality holds, there must exist a directed edge $X \rightarrow Y$ in \mathbb{G} , and the directed edge $X \leftarrow Y$ in $\underline{\mathbb{G}}$.

Let $\mathbf{Q} = \text{Pa}_{\mathbb{G}}(Y) \setminus X$ and $\mathbf{R} = \text{Pa}_{\underline{\mathbb{G}}}(X) \setminus Y$. Set $\mathbf{S} = \mathbf{Q} \cup \mathbf{R}$. Consider $\mathbf{S} = \mathbf{s}$ with $p(\mathbf{s}) > 0$. Let $X^* = (X|\mathbf{S} = \mathbf{s})$ and $Y^* = (Y|\mathbf{S} = \mathbf{s})$. Note that ε_Y and X, \mathbf{S} are d-separated in \mathbb{G} , so $\varepsilon_Y \perp\!\!\!\perp (X, \mathbf{S})$ by the global Markov property. Similarly, ε_X and Y, \mathbf{S} are d-separated in $\underline{\mathbb{G}}$, so $\varepsilon_X \perp\!\!\!\perp (Y, \mathbf{S})$. Peters and colleagues showed that $g(X^*, \mathbf{q}, \varepsilon_Y) \stackrel{d}{=} g(X, \mathbf{Q}, \varepsilon_Y)|\mathbf{s}$ for any measurable function g in their Lemma 36 so long as $p(\mathbf{s}) > 0$ (and likewise for Y^*) [3]. Applying this result gives the bivariate model:

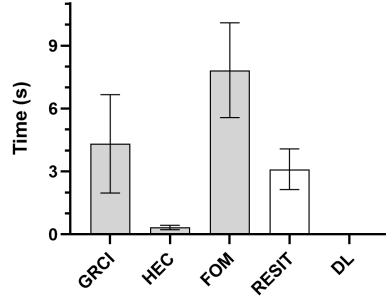
$$\begin{aligned}Y^* &= m_Y(\mathbf{q}, X^*) + \varepsilon_Y \sigma_Y(\mathbf{q}, X^*) \text{ with } \varepsilon_Y \perp\!\!\!\perp X^* \text{ in } \mathbb{G}, \\ X^* &= m_X(\mathbf{r}, Y^*) + \varepsilon_X \sigma_X(\mathbf{r}, Y^*) \text{ with } \varepsilon_X \perp\!\!\!\perp Y^* \text{ in } \underline{\mathbb{G}}.\end{aligned}$$

But we chose \mathbf{s} such that $p(x, y|\mathbf{s})$ does not satisfy Equation (6) – a contradiction of Theorem 1. \square

Additional Timing Results

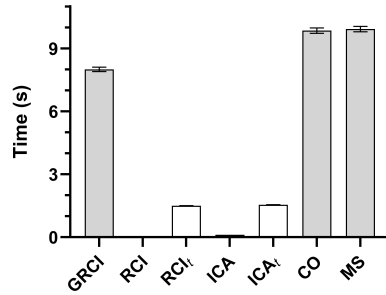


(a) Synthetic pairs

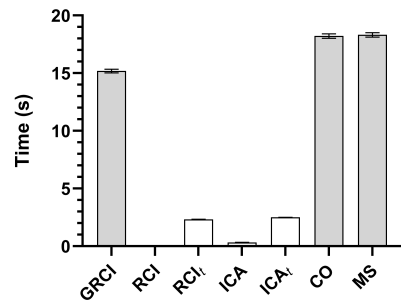


(b) Tübingen cause-effect pairs

Fig. 7: Timing results for the causal direction experiments. HNM-based methods are highlighted in gray. GRCI takes longer than RESIT in (b) because we capped the RESIT sample size at 3000 due to its scaling issues.



(a) Primary Biliary Cirrhosis



(b) Pima Indians Diabetes

Fig. 8: Timing results for the real datasets.